Electrostatic Curved Electrode Actuators

Rob Legtenberg, John Gilbert, Stephen D. Senturia, *Fellow, IEEE*, and Miko Elwenspoek, *Associate Member, IEEE*

***Abstract*— This paper presents the design and performance of an electrostatic actuator consisting of a laterally compliant cantilever beam and a fixed curved electrode, both suspended above a ground plane. A theoretical description of the static behavior of the cantilever as it is pulled into contact with the rigid fixed-electrode structure is given. Two models are presented: a simplified semi-analytical model based on energy methods, and fully three-dimensional (3-D) coupled electromechanical numerical simulations using CoSolve-EM. The two models are in qualitative agreement with each other, and predict stable actuator behavior when the beam deflection becomes constrained by the curved electrode geometry before electrostatic pull-in can occur. The pull-in behavior depends on the shape of the curved electrode. Test devices have been fabricated by polysilicon surface micromachining techniques. Experimental results confirm the basic theoretical results. Stable behavior with relatively large displacements and forces can be generated by these curved electrode actuators. Depending on the design, or as a result of geometrical imperfections, regions of unstable (pull-in) deflection behavior are also observed. [212]**

***Index Terms*—Actuator, electrode shape, electrostatic, theoretical model(ling).**

I. Introduction

ELECTROSTATIC actuation is very attractive for microelectromechanical systems because of good scaling properties to small dimensions, high-energy densities, and relative ease of fabrication. However, electrostatic actuators which are able to generate relatively large displacements and large forces are difficult to design as a result of a geometric discrepancy. Large-displacement actuators (e.g., comb drive structures) require displacements perpendicular to the major field lines, leading to small forces. Large-force actuators (e.g., parallel-plate structures) require small gaps and a displacement in the direction of the major field lines, thus implying small displacements. Several actuator designs have been reported employing curved structures in order to generate large displacement and large forces. A curved electrode has been applied in a microactuator for aligning optical fibers [1]. Actuators have been presented where a large vertical displacement is obtained by an S-shaped film sandwiched between planar electrodes [2]. Another design employs a deformed membrane which is pulled against a glass plate by electrostatic forces [3]. Also, active joints have been proposed that employ a bent beam electrode that is pulled against a rigid counter-electrode [4]. Furthermore, a distributed electrostatic microactuator using wave-like electrodes [5] and an electrostatic moving-wedge actuator for use in a microrelay [6] have been presented. All these actuators use curved structures with a specific shape that are deflected by electrostatic forces toward a counter-electrode, and generate displacements that are normal to the wafer surface.

In order to investigate the basic phenomena of these actuators, the static behavior of cantilever beam structures that are deformed by electrostatic forces along curved electrodes has been studied. Special attention has been given to the effect of the electrode curvature on the static behavior of the actuators. The dynamic properties of comparable structures have been presented elsewhere [7]. Test devices, consisting of a laterally compliant cantilever beam and a fixed curved electrode, both suspended above a ground plane, have been fabricated by polysilicon surface micromachining techniques [8]. Experimental data from these structures are compared with theoretical results.

II. Design

Fig. 1 shows the basic design of the cantilever beam and the curved electrode. The gap distance between electrodes is small near the clamped edge of the beam and increases with the position along the length of the beam. When a voltage is applied across the gap, an electrostatic force is created that deforms the beam along the outline of the curved electrode. The displacement is parallel to the wafer surface. In this way, the shape of the curved electrode can be easily adjusted by changing the mask design. To prevent a short circuit between the beam and the curved electrodes, electrical insulation is required, e.g., by applying a dielectric layer between the structures or by using stand-off bumper structures that prevent physical contact of the electrodes. While this work focuses on cantilever beam structures, similar actuators can be fabricated using microbridges or membranes.

Simple polynomials normalized to the maximum cantilever tip deflection have been used for the shape of the curved electrode $s(x)$ which can be described by the following expression:

$$s(x) = \delta_{\max}\left[\frac{x}{L}\right]^n \tag{1}$$

where $\delta_{\max}$ is the maximum gap distance of the curved electrode, x is the position along the x-axis, L is the length of the beam, and n is the polynomial order of the curve, $n \geq 0$. For different values of n, the electrode shape is shown in Fig. 2. As will be shown in the next section, the performance

Manuscript received May 17, 1996; revised December 4, 1996. Subject Editor, N. de Rooij. This work was supported in part by the Dutch Technology Foundation (STW) and by the Advanced Research Projects Agency under Contract J-FBI-92-196.

R. Legtenberg and M. Elwenspoek are with MESA Research Institute, University of Twente, 7500 AE Enschede, The Netherlands.

J. Gilbert and S. D. Senturia are with the Microsystems Technology Laboratory, Massachusetts Institute of Technology, Cambridge, MA 02139 USA.

Publisher Item Identifier S 1057-7157(97)05809-5.

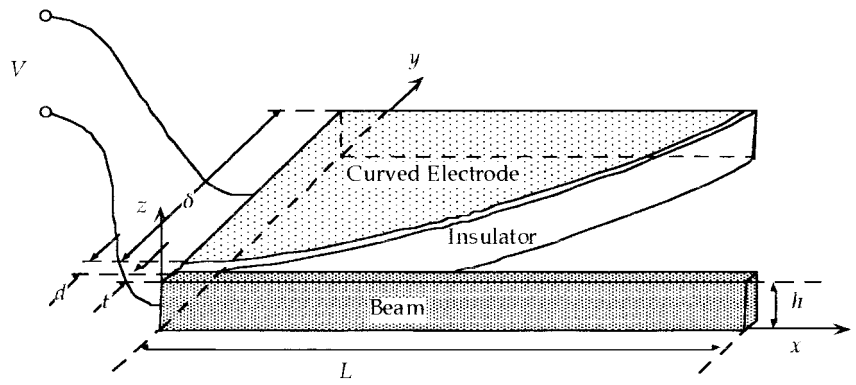

Fig. 1. Schematic view of the curved electrode actuator.

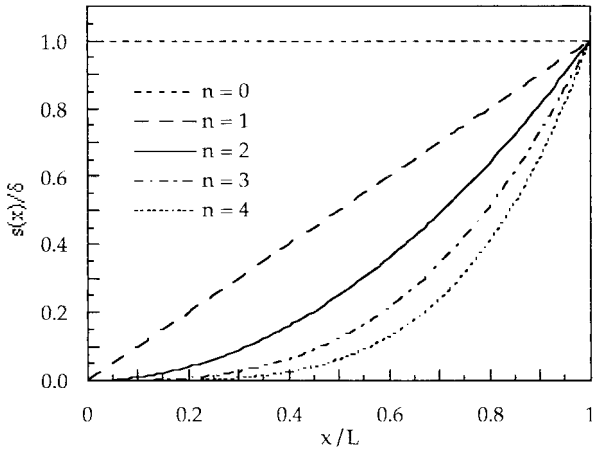

Fig. 2. Normalized graph showing the shape of the curved electrode as a function of x [see (1)].

of these actuators depends on the electrode curvature and can become unstable beyond the so-called pull-in voltage.

III. Actuator Models

Two actuator models are presented. The first is a two-dimensional (2-D) model based on analytical energy methods, supported by numerical determination of required coefficients. Of necessity, this approach requires several major approximations such as the neglect of fringing fields and omission of the effect of the nearby ground plane. The second model is a fully three-dimensional (3-D) self-consistent electromechanical numerical simulation using the MIT MEMCAD System, specifically, the CoSolve-EM module [9]. The energy approach offers the benefit of analytical insight into structural aspects of the design; the 3-D simulations provide the ability to check the energy-model results, and to examine issues not included in the energy model.

A. Energy Model

1) Unloaded and Unconstrained Static Behavior: Because the gap spacing is small with respect to the electrode length it is assumed that the electric field exhibits a one-dimensional (1-D) field line distribution, i.e., a parallel-plate approximation. As stated above, fringing fields are ignored.

When a dc polarization voltage is applied between the capacitor electrodes, an electrostatic force is developed that is inversely proportional to the square of the gap spacing. This makes the force dependent on the deflection, leading to nonlinear behavior. The static deflection $w(x)$ of a prismatic beam with a transverse pressure $q(x,V)$ can be described by the following nonlinear differential equation:

$$EI\frac{d^4w(x)}{dx^4} = q_{(x,V)} = \frac{1}{2}\frac{\varepsilon_0 h V^2}{\left[\frac{d}{\varepsilon_r} + s_{(x)} - w_{(x)}\right]^2} \tag{2}$$

where $q(x,V)$ denotes the static electrostatic force per unit beam length as a function of the position x and the drive voltage V, EI is the bending stiffness, d is the thickness of the insulator, ε_0 the dielectric constant in air, h the width of the beam, ε_r is the dielectric constant of the insulator, and $s_{(x)}$ the shape of the electrode as a function of the position x.

An analytical closed-form solution of the above equation cannot be found. A simplified model is developed based on the Rayleigh–Ritz method with small-deflection theory, where an approximate solution to the differential equation is constructed in the form of admissible trial functions containing undetermined parameters, the parameter values being found by a variational minimization of the total potential energy [10], [11]. The total potential energy, denoted by Π, can be expressed as

$$\Pi = U_b + V_{\text{el}} \tag{3}$$

where U_b and V_{el} are, respectively, the strain energy of bending and the electrostatic potential energy (the first integral of the electrostatic force $q(x,V)$, given by

$$U_b = \frac{1}{2}\int_0^L EI\left[\frac{d^2w_{(x)}}{dx^2}\right]^2 dx \tag{4}$$

and

$$V_{\text{el}} = -\frac{1}{2}\int_0^L \frac{\varepsilon_0 h V^2}{\frac{d}{\varepsilon_r} + s_{(x)} - w_{(x)}}\,dx. \tag{5}$$

The deflection profile of a uniformly loaded cantilever beam has been used for the admissible trial function

$$\tilde{w}(x) = cg(x) = cx^2(6L^2 - 4Lx + x^2) \tag{6}$$

where c is a constant to be determined. This function satisfies the full set of boundary conditions of the beam and is therefore

TABLE I
CALCULATED PULL-IN VOLTAGES FROM THE ENERGY MODEL, FOR POLYSILICON ($Ey = 150$ GPa) CANTILEVER BEAMS ($h^*t^*L = 5^*2^*500$ μm) WITH A MINIMUM GAP SPACING d of 2 μm AND A MAXIMUM DEFLECTION $\delta_{\max}$ of 30 μm. A RELATIVE DIELECTRIC CONSTANT OF THE INSULATOR ε_r EQUAL TO 1 HAS BEEN USED

n	V_{pi} [V]	c_{pi}[$*10^7$ m^{-3}]
0	141.7	7.63
0.5	115.2	7.66
1.0	86.2	7.56
1.5	59.5	6.88
2.0	40.0	5.54

expected to give an excellent correlation between the results from the exact solution of the differential equation and the approximate solution [10].

The system is in equilibrium when the first variation of the total potential energy with respect to the constant c equals zero. Whether this equilibrium is stable or unstable is determined by the second variation of the potential energy with respect to c. At the transition from a stable to an unstable equilibrium both the first and the second derivatives of the potential energy with respect to c are zero. Solving these two equations simultaneously yields the pull-in voltage of the cantilever $V_{\rm PI}$ and an implicit expression for the constant c at pull-in $(c_{\rm PI})$

$$V_{\rm PI}^2 = \frac{EI}{\varepsilon_0 h} \frac{\int_0^L \left[\frac{d^2 g_{(x)}}{dx^2}\right]^2 dx}{\int_0^L \frac{g_{(x)}^2}{\left(\frac{d}{\varepsilon_r} + s_{(x)} - c_{\rm PI}\, g_{(x)}\right)^3} dx} \tag{7}$$

$$\int_0^L \frac{c_{\rm PI} g_{(x)}^2\, dx}{\left(\frac{d}{\varepsilon_r} + s_{(x)} - c_{\rm PI}\, g_{(x)}\right)^3} = \int_0^L \frac{g_{(x)}\, dx}{\left(\frac{d}{\varepsilon_r} + s_{(x)} - c_{\rm PI}\, g_{(x)}\right)^2}. \tag{8}$$

The calculated pull-in voltages for different polynomial orders obtained by this energy method are listed in Table I.

Equations (7) and (8) give little insight in the effect of different parameters. Some aspects will be discussed here. Increasing the polynomial order n of the electrode curve decreases the pull-in voltage while the maximum displacement just before pull-in stays about the same. Thus by using curved electrodes, the pull-in voltage can be lowered significantly, resulting in large amplitude motion at lower driving voltages as compared to a parallel-plate structure $(n = 0)$. At voltages above the pull-in voltage, the displacement cannot be controlled because of the unstable pull-in event. The maximum tip displacement at pull-in is independent of the beam properties and only depends on the gap geometry. The tip displacement at pull-in, calculated from the examples in Table I, is about one third of the maximum gap spacing $d_{\max}$ which is comparable to the behavior of a lumped parallel-plate spring model (see, for example, [12]). The pull-in voltage strongly decreases either with decreasing initial gap spacing at the clamped edge of the beam or with increasing dielectric constant of the insulating layer between the electrodes.

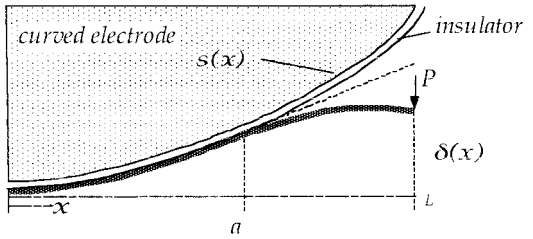

Fig. 3. Sketch of the constrained beam deflection model with external loading force P.

2) Constrained Static Behavior: The pull-in voltage decreases with increasing polynomial order. However, for polynomial orders above two it was found that the deflection profile of the beam becomes constrained by the geometry of the curved electrode before the pull-in voltage is reached. For this situation, the model needs to be adjusted. In addition, a force P, that is acting on the tip of the beam, has been added in order to perform external work. This force will deform the beam wherever it is not yet in contact with the curved electrode.

It is assumed that the beam will be partly in contact with the curved electrode and will partly be free standing and is clamped at point a, as sketched in Fig. 3. The problem will thus have a variable-boundary condition with respect to the free-standing length of the beam. Therefore, the system must be divided into two regions. From the clamped edge of the beam to point a the beam is assumed to be in physical contact with the curved electrode. Thus the deflection profile $w_{(x)}$ will be equal to the shape of the electrode $s_{(x)}$ and the distance between the electrodes is equal to d, the thickness of the insulator. Beyond point a, the beam is free and is deflected by electrostatic forces and by the external force P.

The expressions for the strain energy of bending and the electrostatic potential energy become

$$U_b = \frac{1}{2}\int_0^a EI\left[\frac{d^2 s_{(x)}}{dx^2}\right]^2 dx + \frac{1}{2}\int_a^L EI\left[\frac{d^2 w_{(x)}}{dx^2}\right]^2 dx \tag{9}$$

and

$$V_{\rm el} = -\frac{1}{2}\int_0^a \frac{\varepsilon_r \varepsilon_0 h V^2}{d}\, dx - \frac{1}{2}\int_a^L \frac{\varepsilon_0 h V^2}{\frac{d}{\varepsilon_r} + s_{(x)} - w_{(x)}}\, dx. \tag{10}$$

An additional term, the work from the external force acting on the tip of the beam, must be added to the total potential energy [see (3)], and is given by

$$V_P = P w(L). \tag{11}$$

The admissible trial function of the deflection profile of the cantilever beam now also depends on the contact distance a and applied force P

$$\tilde{w}_{(x)} = s_{(x)}, \qquad \text{for } 0 < x \le a \tag{12}$$

$$\tilde{w}_{(x)} = c(x-a)^2[6(L-a)^2 - 4(L-a)(x-a) + (x-a)^2] - \frac{P(x-a)^2[3(L-a) - (x-a)]}{6EI} + \left[s_{(x)}\right]_{x=a} + \left[\frac{ds}{dx}\right]_{x=a}(x-a), \qquad \text{for } a < x < L. \tag{13}$$

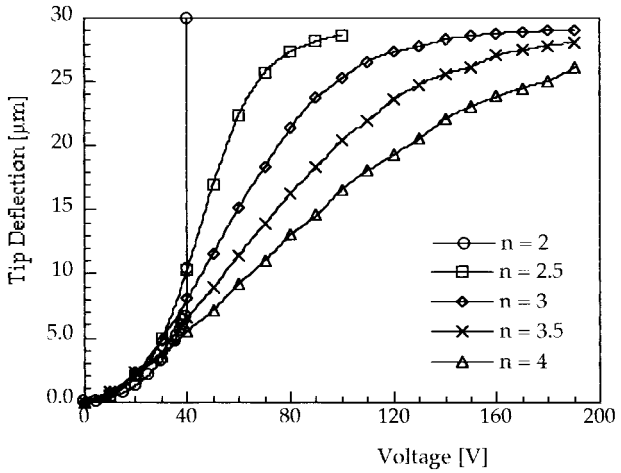

Fig. 4. Modeled tip deflection as a function of the applied voltage for several polynomial orders n of the curved electrode. When the polynomial order is larger than 2 the behavior becomes stable up to the maximum tip deflection. Otherwise, a pull-in voltage exists. Variable settings that have been used are: $E_y = 150$ GPa, $h = 5$ μm, $t = 2$ μm, $L = 500$ μm, $d = 2$ μm, $\delta_{\max} = 30$ μm, and $\varepsilon_r = 1$.

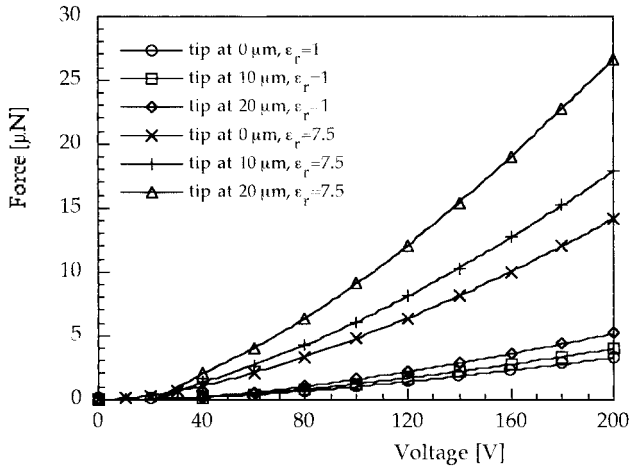

Fig. 5. Theoretical force generation of a quadratic order electrode curvature as a function of driving voltage. The tip deflection is fixed at 0, 10, and 20 μm. Also the effect of the relative dielectric constant of the insulating layer is shown. Unless given in the graph, variable settings equal to Fig. 4 have been used.

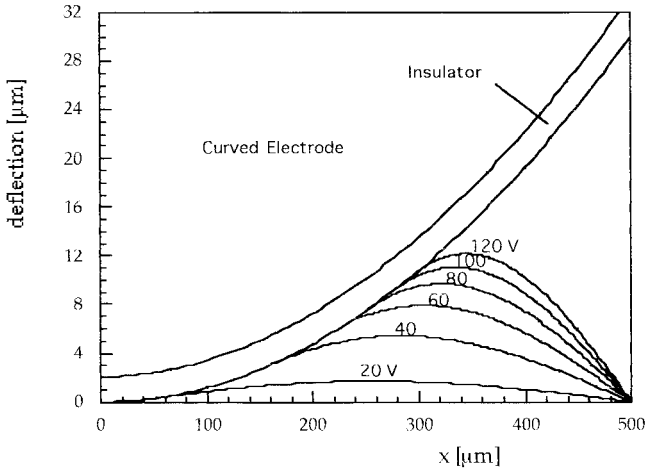

Fig. 6. Deflection profiles of the cantilever beam in Fig. 5 for several driving voltages when the tip is constrained at zero deflection.

This system is in equilibrium when the first variation of the potential energy with respect to the contact distance a equals zero and the first variation of the potential energy with respect to the constant c equals zero. Solving both equations simultaneously by numerical iteration gives the values of a and c at any given applied voltage.

The tip deflection versus driving voltage for unloaded designs with a polynomial order ranging from two to four is shown in Fig. 4. For designs with a polynomial order above 2, stable behavior (no pull-in) up to the maximum tip deflection is found. This is the result of the constrained beam deflection which makes the beam zip along the curved electrode as the voltage is increased.

The boundary between constrained and unconstrained behavior can be more easily understood when only the collapsed part of the beam is considered (i.e., $x \leq a$). In that case, only the first terms on the right-hand side of (9) and (10) are considered. The dependency of the system on the polynomial order n can be found by looking at the first and second derivatives of the total potential energy with respect to this polynomial order n. A short mathematical exercise which, for the sake of brevity, is not included here shows that; the second derivative of the total potential energy with respect to the polynomial order n for this simplified situation becomes negative for $n < 2$ indicating unstable behavior; the second derivative of the total potential energy with respect to n is zero for $n = 2$ indicating an extremum; and that the second derivative of the potential energy with respect to n becomes positive $n > 2$ indicating stable behavior.

3) Force Generation: The force generated by the actuator is a function of the displacement of the tip. It can be found numerically by setting the first variations of the potential energy with respect to the contact distance a and the constant c to zero at an assumed tip displacement. The resulting external force as a function of tip position is shown in Fig. 5. Actuator dimensions are given in the figures; the effect of the dielectric constant of the insulating layer between the electrodes is also shown. Forces are typically a few micronewtons for this example but increase with decreasing gap distance and with increasing dielectric constant of the insulating layer. The deformation of the beam is illustrated in Fig. 6, for the case of the tip fixed at zero deflection. When the actuator is loaded by displacement-dependent forces, for example, a spring, the problem can be solved by substitution of the appropriate force-displacement relation.

B. 3-D Coupled Electromechanical Simulations

In order to study 3-D effects like fringing fields and the effect of the ground plane (see Fig. 7), simulations have been performed using CoSolve-EM [9]. CoSolve-EM is a software package that is capable of doing self-consistent electromechanical analysis of complex 3-D structures. The approach is based on a relaxation scheme combining a fast multipole-accelerated scheme for the electrostatic analysis (FASTCAP [13]) with a standard finite-element method for the mechanical system analysis (ABAQUS [14]).

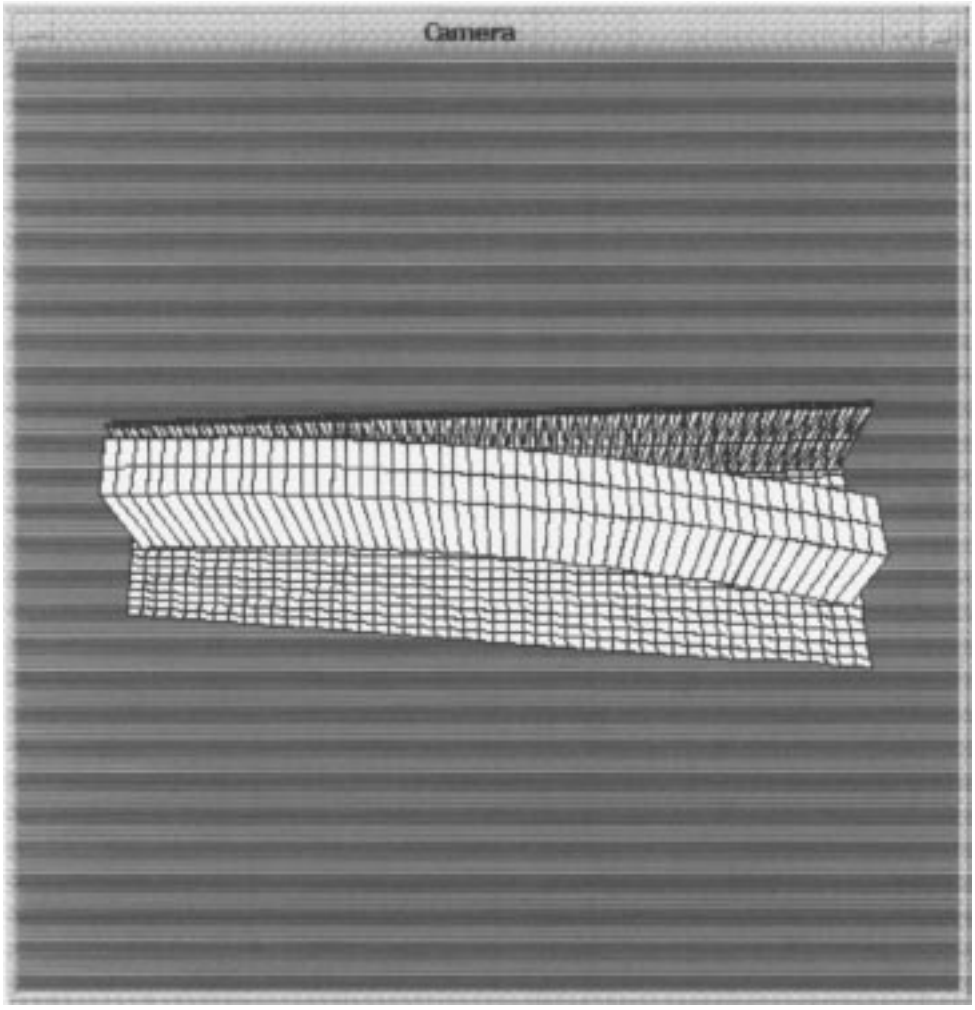

Fig. 7. Example of a geometric model used in the CoSolve-EM simulations (order $= 2$).

In the model of Fig. 7, x is along the length of the beam, z is in a direction normal to the ground plane, and the principal motion of the beam is in y-direction toward the curved electrode. Because the cantilever beam contacts the curved electrode, an interface had to be inserted between the electrodes using CoSolve-EM. And because of convergence problems in the presence of contact with the present version of CoSolve-EM, the levitation in z direction of the beam, which results from a lack of balance between fringing-field forces on the top and bottom surfaces of the cantilever, had to be suppressed [9]. The calculated tip deflection versus driving voltage for quadratic, cubic, and fourth-order electrode curvatures with an initial gap distance of 1 μm are shown in Fig. 8, together with results from the energy model.

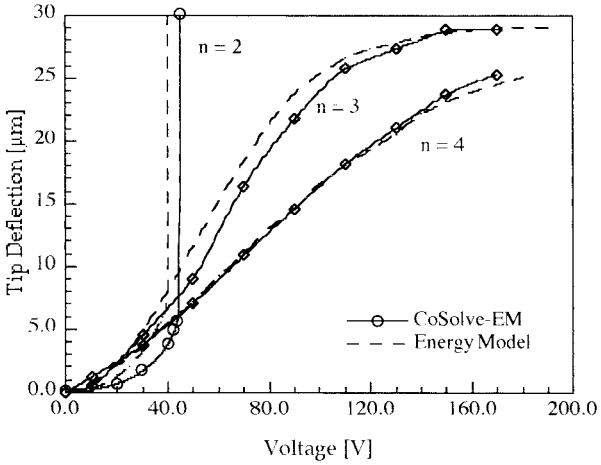

Fig. 8. Results of the unloaded tip deflection versus voltage behavior for the energy model using a parallel-plate approximation and the 3-D finite-element model in the presence of the ground plane. The dielectric constant of the spacer is 1, and a Youg's modulus E_y of 150 GPa, a Poisson's ratio ν of 0.3, beam dimensions $(h * t * L)$ of $5 * 2 * 500$ μm, a minimal gap spacing d of 2 μm, and maximum gap spacing $\delta_{\max}$ of 30 μm have been used in the calculations.

It can be concluded that the results from the energy model and the 3-D coupled electromechanics are qualitatively in good agreement with each other. But there are two effects which compete. The energy model neglects fringing fields. Therefore, one would expect the 3-D simulations, which add the fringing fields to the problem, to show larger displacements and lower pull-in voltages. However, comparing the two models suggests the opposite, reduced tip displacements and increased pull-in voltage compared to the energy model. It is readily shown from a comparison of 3-D simulations with and without the ground plane that if fringing fields are included, then the effect of

the ground plane is to significantly reduce the contribution of these fringing fields to the actuation force. However, because levitation was suppressed in these simulations, and because levitation will also reduce the actuation force, it is not yet possible to resolve unambiguously the two effects of the ground plane (reducing fringing and causing levitation).

As discussed below, some of the fabricated actuators employ polysilicon bumper structures instead of a continuous insulating layer between the electrodes to simplify the fabrication process. The static behavior of these complex structures can easily be simulated by CoSolve-EM by attaching interface nodes at the corresponding bumper positions. Results of this type are presented in the section on experimental results of constrained bumper designs.

IV. Fabrication

A one mask fabrication process has been developed where electrical insulation between the electrodes is obtained by polysilicon bumper structures or by a sidewall silicon nitride layer.

The fabrication starts with a (100) p-type 3-in silicon wafer. The first step is wet thermal oxidation at 1150 °C to obtain a 2-μm-thick SiO_2 sacrificial layer. Next, a 5-μm-thick polysilicon layer is grown by LPCVD at a temperature of 590 °C, a pressure of 250 mtorr, and a silane flow of 50 sccm. This polysilicon layer is heavily doped with boron by deposition of a BSG layer and indiffusion at 1150 °C for 3 h. This yields a sheet resistance of about 4.5 Ω/square and also results in a small residual strain and strain gradient of the polysilicon layer [15]. The residual stress in the polysilicon is in the order of only 20 MPa, but will completely disappear once the cantilever beams are etched free. After boron indiffusion, the BSG layer is stripped in a buffered HF solution. A 0.6-μm-thick PECVD SiO_2 layer is grown that serves as an etch mask for the polysilicon. After patterning this SiO_2 layer by RIE using CHF_3 gas, the polysilicon is anisotropically etched using a SF_6, O_2, CHF_3 gas mixture. This anisotropic etching process results in almost perfectly vertical sidewalls [16]. After a cleaning step, the sacrificial layer is etched in a buffered HF solution for 30 min. This only frees the thin beams but leaves the larger structures attached to the substrate. Drying is done by means of a special freeze-drying method to prevent stiction of free structures to the substrate [15]. Finally, a 1-μm-thick aluminum layer is evaporated for backside contact. The final result for bumper designs is shown in Fig. 9.

By introducing a deposition of LPCVD low-stress silicon nitride after anisotropically etching the polysilicon and a subsequent anisotropic RIE step in CHF_3 gas, silicon nitride sidewall layers are obtained that act as a continuous insulating layer between the electrodes. Examples of devices having silicon nitride sidewall insulation are shown in Fig. 10.

V. Experimental Results and Discussion

A. Experimental Setup

The tip deflection as a function of the applied driving voltage has been measured for different electrode curves using a probe station with a microscope and a digital voltage supply. The beam electrode and the substrate are connected to a ground potential while the curved electrode is connected to a positive voltage. Deflections and dimensions have been measured using a micrometer eyepiece with an accuracy of, respectively, $\pm$ 0.3 μm and $\pm$ 0.1 μm.

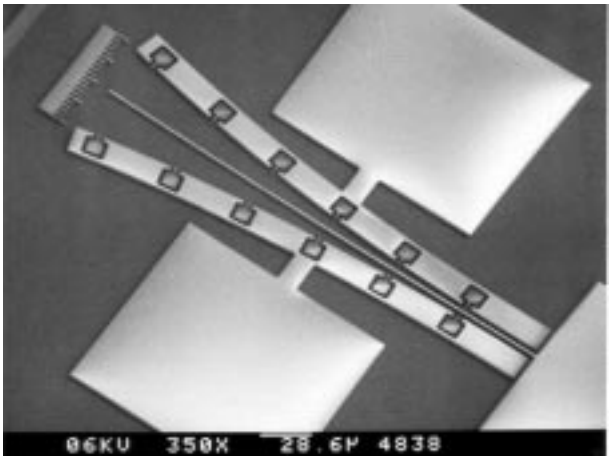

(a)

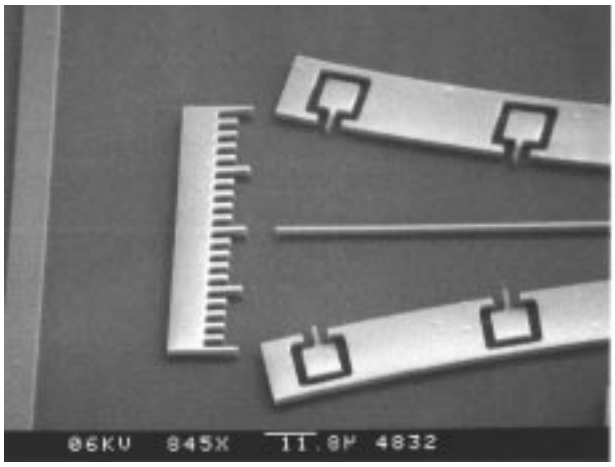

(b)

Fig. 9. (a) SEM photograph of curved electrode actuator with stand off bumpers (order = 3). (b) Closeup of the free-standing actuator tip and the stand-off bumper structures.

B. Pull-in Voltage of Instable Bumper Designs

To determine the pull-in voltage, the driving voltage was slowly increased until the observed beam deflection became unstable. The results are shown in Fig. 11 and the pull-in voltages are listed in Table II. The calculated pull-in voltages as obtained from the energy model are smaller than the measured values. The difference grows with decreasing order of the electrode curvature. This can be explained by 3-D electrostatic field effects. Electrostatic fringing fields will increase the electrostatic forces and will result in lower pull-in voltages than calculated by our simple parallel-plate approximation. However, the presence of the groundplane gives rise to an unbalanced electrostatic field distribution [17]. This effect reduces the electrostatic forces, especially for large gaps, and induces a levitation of the surface mi-

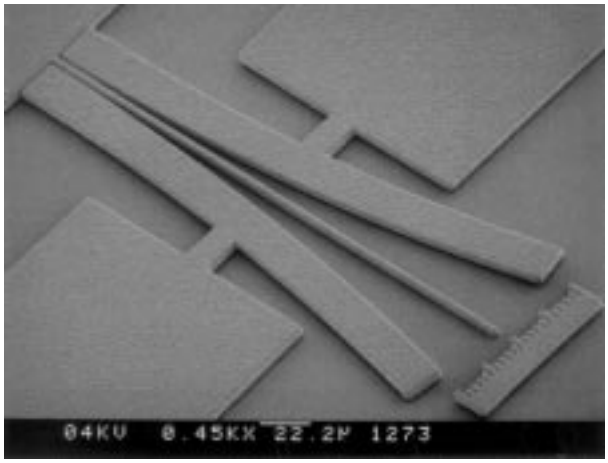

(a)

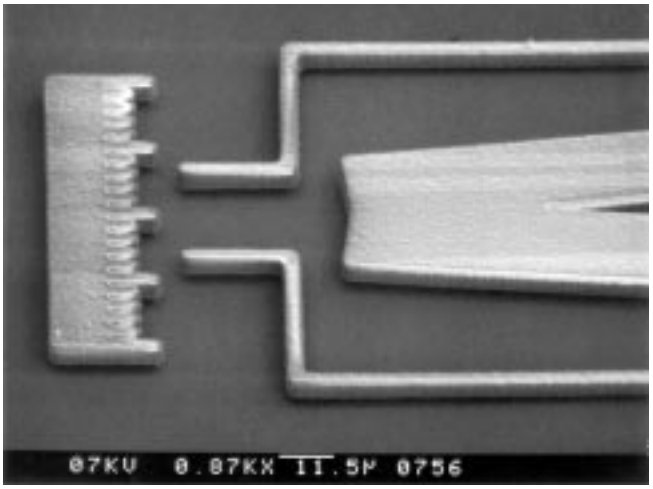

(b)

Fig. 10. (a) SEM photograph of curved electrode actuator with a silicon nitride sidewall insulation. (b) SEM photograph of a microgripper employing curved electrode structures for actuation.

cromachined structure. The pull-in voltage will increase by the presence of the ground plane and this effect will be stronger for increasing gap distances. Therefore, it is difficult to give accurate quantitative predictions of the pull-in voltage by a simple 1-D model. The calculated pull-in voltages that are obtained from the 3-D coupled solver are in better agreement with our experimental results. The aforementioned 3-D effects are now clearly incorporated in the simulations. Note that the pull-in voltage is very sensitive to the thickness of the cantilever beam and the initial gap spacing. For instance, the measurement error in the beam thickness of $\pm 0.1\,\mu$m results in a change of about $\pm 10\%$ in the pull-in voltage of a second-order polynomial design.

The behavior of the actuators shows a hysteresis effect for increasing and decreasing voltages. This has been studied in more detail for the second-order polynomial electrodes. The experimental results are shown in Fig. 12. The origin of the hysteresis comes from a difference in the electrostatic field distribution between a beam before and after pull-in. Once the beam is collapsed, the electrostatic forces strongly increase as a result of the decreased gap spacing and a large decrease in the driving voltage is needed before bending forces overcome the electrostatic forces again.

TABLE II

PULL-IN VOLTAGE OF POLYSILICON ($E_y = 150$ GPa) CANTILEVER BEAMS USING BUMPER STRUCTURES WITH A MAXIMUM DEFLECTION $\delta_{\max}$ OF 30 μm. THE MEASURED THICKNESS OF THE POLY LAYER IS 4.6 μm (WIDTH OF THE BEAM), THE THICKNESS OF THE SACR.IFICE LAYER IS 1.6 μm. THE THICKNESS T OF THE DIFFERENT BEAMS IS 1.6, 1.7, AND 1.8 μm, AND THE INITIAL GAP IS 2.2, 3.2, AND 3.3 μm FOR THE 0, 1, AND 2 ORDER POLYNOMIAL DESIGNS, RESPECTIVELY

order	Pull-in Voltage [V]		
	Cantilever		
	Exp.	CoSolve-EM	Energy
0	223	convergence problems	112
1.0	98	105-107.5	74
2.0	40	37.5-40	37

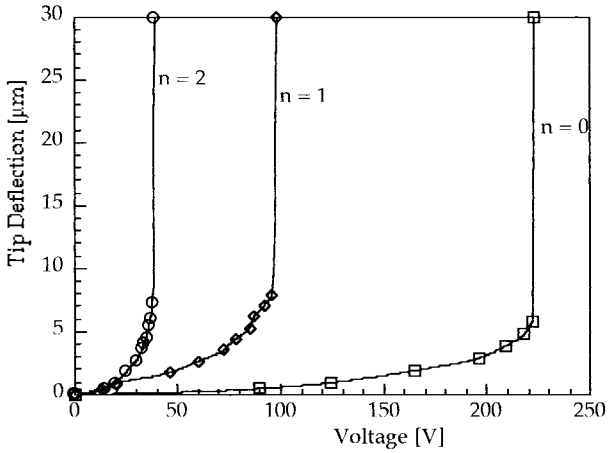

Fig. 11. Measured tip deflection versus driving voltage for unstable electrode profiles. The polynomial orders are 2, 1, and 0. Measured dimensions are given in Table II.

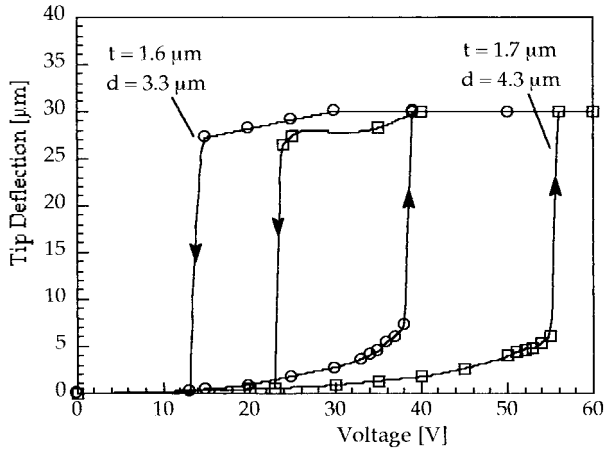

Fig. 12. Measurement of the hysteresis effect for second-order polynomial designs. Beam length and width are, respectively, 500 μm and 4.6 μm. Beam thickness and initial gap spacing are 1.6, 3.3 μm and 1.7, 4.3 μm, respectively.

C. Constrained Bumper Designs

When the polynomial order becomes larger than 2, the deflection of the beam becomes constrained by the geometry

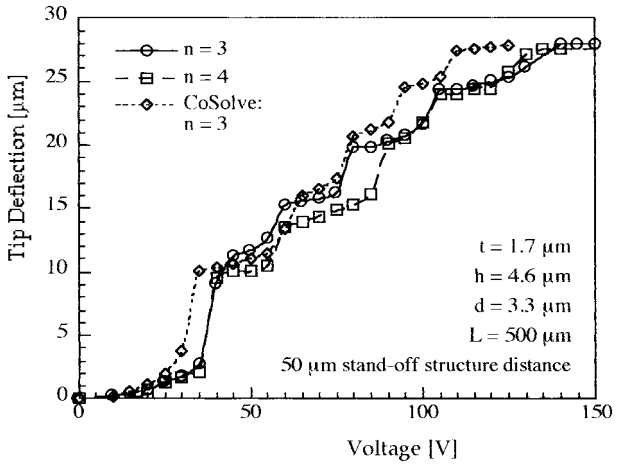

Fig. 13. Experimental results of curved electrodes with stand-off bumper structures where the beam deflection becomes constrained by the electrode geometry (bumpers). The polynomial orders are 3 and 4. Also the results of a CoSolve-EM simulation for a cubic electrode design with a gap spacing of 3.1 μm employing bumper structures spaced apart at every 50 μm and 2 μm away from the curved electrode are shown.

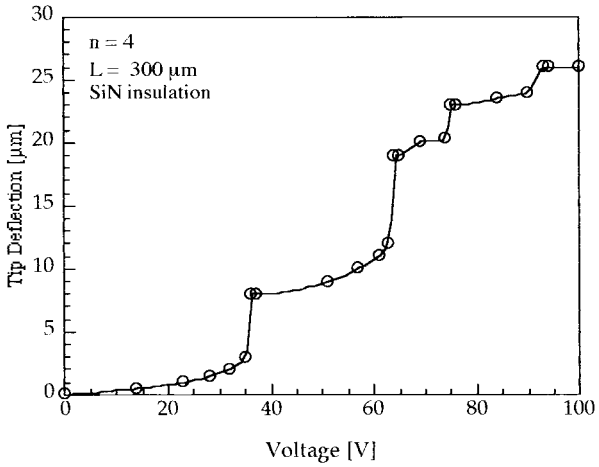

Fig. 14. Example of the measured tip deflection as function of the driving voltage for a fourth-order design with a silicon nitride sidewall layer.

of the curved electrode as discussed earlier. The measured deflection behavior of a third- and fourth-order polynomial curvature design with bumper structures at every 50 μm is shown in Fig. 13 for beams with a length of 500 μm. The use of bumpers results in a stepwise behavior in which the cantilever beam reaches an unstable point from bumper to bumper. Fig. 13 also shows simulated results for the third-order design obtained from CoSolve-EM. The model is in fair agreement with the data. The CoSolve model systematically overestimates the force applied to the beam, possibly a result of the suppression of the levitation.

D. Constrained Sidewall Insulator Designs

An example of the measurement results from an actuator with continuous sidewall insulation is shown in Fig. 14. In contrast to our theoretical results, devices with a continuous sidewall insulator did not show completely stable behavior. Fabricated devices show a behavior that is more or less identical to the constrained bumper designs. Step-like unstable and stable regions are observed. Furthermore, a large variation in behavior of identical designs has been observed.

It is suggested that these results are caused by imperfections at the sidewall surfaces, for example, surface asperities, and entrapped particles or residues between the electrodes after the fabrication process. A close-up view of a beam with sidewall SiN insulation is shown in Fig. 15. The small protrusions could act like small bumpers, preventing the movable beam from smoothly zipping along the curved electrode. For successful constrained designs, smooth electrode surfaces may be required, which may be difficult to realize by the type of fabrication process used here.

Another possibility may be caused by the levitation effect. As the beam zips along the curved electrode, the beam in the first instance will be levitated, and as it zips further along the curved electrode, it will be pulled down again. This up and down movement together with frictional forces, inducing a stick-slip behavior, may also be responsible for the observed

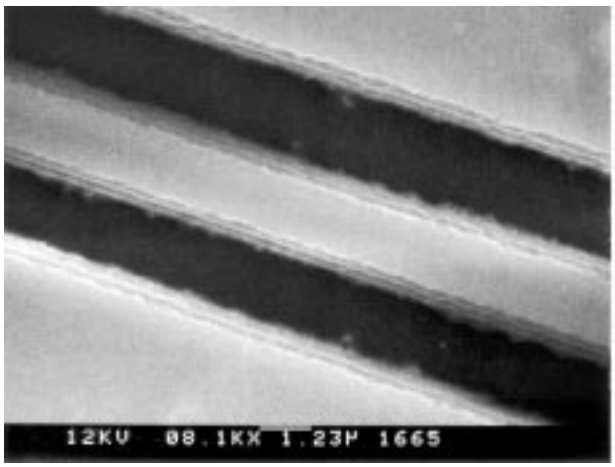

Fig. 15. Closeup SEM top view of a cantilever beam with silicon nitride sidewall passivation. The presence of relative large surface roughness, residue and particles may possibly induce instabilities in the actuator behavior.

results.

VI. Conclusion

An electrostatic actuator design has been presented where a deformable mechanical structure is bent around a fixed curved electrode by means of electrostatic forces. Such a design is attractive because relatively large deflections and forces can be obtained.

Simple polynomials have been used for the shape of the curved electrodes. A theory based upon energy methods was presented to describe the static behavior of the actuator. 3-D coupled electromechanical simulations using CoSolve-EM have been performed. The results from both models are in qualitative agreement with each other. When the beam deflection is not constrained by the curved electrode geometry, unstable behavior occurs at a certain pull-in voltage, and there is hysteresis on release of the structure after pull-in. For polynomial designs with an order above two, it was found that the beam deflection becomes constrained by the curved electrode geometry before pull-in occurs. Our models predict completely stable behavior in this situation.

Curved electrode actuators have been fabricated from polysilicon by surface micromachining techniques using a one-mask process. Electrical insulation has been realized both by stand-off bumper structures between the movable beam and the fixed electrode and by a silicon nitride sidewall layer. Measurements of nonconstrained beam deflections show that the qualitative behavior of the energy model is in agreement with theory but that the pull-in voltages are higher than theoretically predicted. This effect is a result of the presence of a ground plane as shown in 3-D coupled electromechanical simulations which are in good agreement with measurements.

Constrained designs employing bumper structures show a stepwise behavior as a result of constrained motion at the bumper positions. The static behavior of these designs has been modeled by CoSolve-EM and was found to be in fair agreement with experimental data.

Experimental data of samples with a continuous sidewall insulator did not show stable behavior up to maximal deflection, in contrast to our theoretical results. It is suggested that this is caused by imperfections at the sidewall surfaces as a result of the fabrication process, which prevent the movable beam from smoothly zipping along the curved electrode, acting like small bumpers leading to local instabilities.

Curved electrode structures are therefore mainly suited for bistable actuator applications like, for example, microswitches, microgrippers, microvalves, and micropumps.

ACKNOWLEDGMENT

The authors wish to thank B. Geyselears and P. Osterberg for helpful discussions on, respectively, the energy model and the 3-D model generation. They are also grateful to N. van Dellen for doing part of the measurements. Furthermore, they would like to thank B. Otter for making the SEM photographs.

REFERENCES

[1] R. Jebens, W. Trimmer, and J. Walker, "Microactuators for aligning optical fibers," *Sens. Actuators*, vol. 20, pp. 65–73, 1989.

[2] K. Sato and M. Shikida, "Electrostatic film actuator with large vertical displacement," in *Proc. IEEE Conf. on Micro Electro Mechanical Syst.*, Travemunde, Germany, Feb. 4–7, 1992, pp. 1–5.

[3] J. Branebjerg and P. Gravesen, "A new electrostatic actuator providing improved stroke length and force," in *Proc. IEEE Conf. on Micro Electro Mechanical Syst.*, Travemunde, Germany, Feb. 4–7, 1992, pp. 6–11.

[4] M. Elwenspoek, L. Smith, and B. Hök, "Active joints for microrobot limbs," *J. Micromech. Microeng.*, vol. 2, pp. 221–223, 1992.

[5] M. Yamaguchi, S. Kawamura, K. Minami, and M. Esashi, "Distributed electrostatic micro actuator," in *Proc. IEEE Conf. on Micro Electro Mechanical Syst.*, Fort Lauderdale, FL, Feb. 7–10, 1993, pp. 18–23.

[6] J. Schimkat, L. Kiesewetter, H. J. Gevatter, F. Arndt, A. Steckenborn, and H. F. Schlaak, "Moving wedge actuator: An electrostatic actuator for use in microrelay," in *Proc. 4th Int. Conf. and Exhibition on Micro Electro, Opto Mechanical Syst. and Components*, Berlin, Germany, Oct. 19–21, 1994, pp. 989–996.

[7] M. Elwenspoek, M. Weustink, and R. Legtenberg, "Static and dynamic properties of active joints," in *Proc. 8th Int. Conf. on Solid-State Sensors and Actuators*, Stockholm, Sweden, June 25–29, 1995, pp. 412–415.

[8] R. Legtenberg, E. Berenschot, M. Elwenspoek, and J. Fluitman, "Electrostatic curved electrode actuators," in *Proc. IEEE Conf. on Micro Electro Mechanical Syst.*, Amsterdam, The Netherlands, Jan. 29–Feb. 2, 1995, pp. 37–42.

[9] J. R. Gilbert, R. Legtenberg, and S. D. Senturia, "3D coupled electromechanics for MEMS: Applications of CoSolve-EM," in *Proc. IEEE Conf. on Micro Electro Mechanical Syst.*, Amsterdam, The Netherlands, Jan. 30–Feb. 2, 1995.

[10] I. H. Shames and C. L. Dym, *Energy and Finite Element Methods in Structural Mechanics*. New York: McGraw-Hill, 1985.

[11] H. Tilmans and R. Legtenberg, "Electrostatically driven vacuum encapsulated polysilicon resonators—Part II," *Sens. Actuators*, vol. A45, pp. 67–84, 1994.

[12] P. Osterberg, H. Yie, X. Cai, J. White, and S. Senturia, "Self consistent simulation and modeling of electrostatically deformed diaphragms," in *Proc. IEEE Conf. on Micro Electro Mechanical Syst.*, Oiso, Japan, Feb. 25–28, 1994, pp. 28–32.

[13] K. Nabors and J. White, "FastCap: A multipole-accelerated 3-D capacitance extraction program," *IEEE Trans. Computer-Aided Design*, vol. 10, pp. 1447–1459, 1991.

[14] *ABAQUS Manual*, Hibbitt, Karlsson and Sorenson, 1080 Main Street, Pawtucket, RI 02860 USA.

[15] R. Legtenberg, "Electrostatic actuators fabricated by surface micromachining techniques," Ph.D. dissertation, Univ. Twente, Enschede, The Netherlands, 1996.

[16] R. Legtenberg, H. Jansen, M. de Boer, and M. Elwenspoek, "Anisotropic reactive ion etching of silicon using $SF_6/O_2/CHF_3$ gas mixtures," *J. Electrochem. Soc.*, vol. 142, pp. 2020–2028, 1995.

[17] W. C. Tang, M. G. Lim, and R. T. Howe, "Electrostatic comb drive levitation and control method," *J. Micro Electro Mech. Syst.*, vol. 1, pp. 170–174, 1992.

Rob Legtenberg, for a photograph and biography, see this issue, p. 240.

John Gilbert, photograph and biography not available at the time of publication.

Stephen D. Senturia (F'93), photograph and biography not available at the time of publication.

Miko Elwenspoek (A'95), for a biography, see this issue, p. 241.